Interior of the Moon

R. C. Weber

Abstract

A variety of geophysical measurements made from Earth, from spacecraft in orbit around the Moon, and by astronauts on the lunar surface allow us to probe beyond the lunar surface to learn about its interior. Similarly to the Earth, the Moon is thought to consist of a distinct crust, mantle, and core. The crust is globally asymmetric in thickness, the mantle is largely homogeneous, and the core is probably layered, with evidence for molten material. This chapter will review a range of methods used to infer the Moon's internal structure, and briefly discuss the implications for the Moon's formation and evolution.

Key Words: Moon, lunar interior, lunar formation, lunar geophysics, core structure

1. Introduction

Understanding the internal structure of the Moon is of key importance to deciphering its early history. The current consensus is that the Moon formed following the collision of a Mars-sized body with the Earth about 4.5 billion years ago. The rocky mantle of the impactor spun out to form the Moon, while the core of the impactor fell into the growing Earth. This model explains the high spin of the Earth–Moon system, the low density of the Moon relative to the Earth, and the Moon's depletion of lighter **volatile** elements, which were likely ejected during the impact event. The model also provides a source of energy to melt the early Moon.

The geochemical and petrological evidence strongly supports the theory that the molten Moon floated an anorthositic crust about 4.45 billion years ago. This forms the present high-**albedo** highland crust. As the initially hot, molten Moon cooled, the mantle likely crystallized into a sequence of mineral **zones** by about 4.4 billion years ago. Heavier elements sank to form a small metallic core. Following the formation of the crust, major impacts on the surface produced many craters and multi-ring basins, probably during a spike or "cataclysm" around 3.9 – 4.0 billion years ago. The oldest basin observed is the South Pole – Aitken Basin and the youngest is the Orientale Basin, which formed 3.85 billion years ago.

Beginning about 4.3 billion years ago, and peaking between 3.8 and 3.2 billion years ago, partial melting occurred in the lunar interior, and basaltic lavas flooded the low-lying basins on the surface. This occurred mostly on the nearside, where the crust is thinner, resulting in the low-albedo lunar mare. Major volcanic activity ceased around 3.0 billion years ago, although minor activity may have continued until 1.0 – 1.3 billion years ago. The Moon has suffered only a few major impacts since that time (forming, for example, the young **rayed** craters such as Copernicus and Tycho).

An overview of the commonly-accepted model of the Moon's present day internal structure, illustrating the crust, mantle, and core layers, is shown in Figure 1, and includes the probable depths of the interfaces between the core layers.

2. Bulk lunar properties

The mass of the Moon, determined from the orbital periods of various spacecraft using **Kepler's third law**, is 7.35×10^{22} kg, which is 1/81 of the mass of the Earth. Although the Galilean satellites of Jupiter (Io, Europa, Ganymede, and Callisto), and Saturn's moon Titan are comparable in mass, the Moon/Earth ratio is the largest satellite-to-parent mass ratio in the solar system (Table 1). The lunar radius is 1738 ± 0.1 km, or 27% of the Earth's radius. This radius is intermediate between that of Europa (radius = 1561 km) and Io (radius = 1818 km). The Moon is much smaller than Ganymede (radius = 2634 km), which is the largest satellite in the solar system. The lunar mean density is 3.344 ± 0.003 g/cm^3, while the Earth has a much higher mean density of 5.52 g/cm^3. The lunar density is also intermediate between that of Europa (density = 3.014 g/cm^3) and Io (density = 3.529 g/cm^3). Most of the other known satellites in the solar system are ice-rock mixtures and so are much less dense.

The Moon's moments of inertia (MOI) are related to its second-degree gravitational harmonics, which have been measured to high precision by orbiting spacecraft. Current estimates indicate that the Moon's mean MOI is 0.3931 ± 0.0002, very close to that of a uniform density sphere, which has a moment of inertia of 0.4. This requires a slight density increase toward the center of the Moon, in addition to the presence of a low-density crust. In comparison, the mean MOI value for the Earth, with its dense metallic core that constitutes 32.5% of the Earth's total mass, is 0.3315.

The mass of the Moon is distributed in a nonsymmetrical manner, with the center of mass (CM) lying 1.8 km closer to the Earth than the geometrical center of figure (CF) (Figure 2). This offset is due to the presence of a thicker farside crust. This is a major factor in placing the Moon into synchronous orbit with the Earth, such that the Moon always presents the same face to the Earth. The gravitational influence of the Earth (and to a lesser extent, the Sun) on the Moon's asymmetric mass distribution resulted in torques that slowed down the rotation of the early Moon, until it became tidally locked. However, the lunar longitudinal and latitudinal **librations** in combination allow a total of 57% of the Moon's surface to be visible at different times in the orbital cycle.

Various explanations have been advanced to account for the offset of the Moon's center of mass from its center of figure. Dense mare basalts erupted from the lunar interior cover about 17% of the lunar surface, mostly on the nearside, but they are usually less than 1 or 2 km thick and constitute only about 1% of the total volume of the crust – insufficient by about an order of magnitude to account for the effect. It has also been suggested that the offset could arise if the lunar core is displaced from the center of mass. However, such a displacement would generate shear stresses that could not be supported by the hot, likely molten (or partially molten) deep interior. Another suggestion is that some form of density asymmetry developed in the mantle during crystallization of the magma ocean, with a greater thickness of lower density materials

being concentrated within the farside mantle. However, it is unlikely that such density irregularities would survive stress relaxation in the hot interior, unless actively maintained by convection (for which there is no present-day evidence).

The conventional explanation for the CM/CF offset is that the farside highland low-density crust is thicker, probably a consequence of an asymmetry developed during crystallization of the magma ocean. This explanation is supported by crustal thickness estimates derived from gravity mapping (see Section 3.2). The crust is massive enough and sufficiently irregular in thickness to account for the CM/CF offset. An equipotential surface is closer to the actual surface on the nearside. Magmas that originate at equal depths below the surface will thus have greater difficulty in reaching the surface on the farside, where the crust is thicker. This explains the scarcity of observed mare basalts on the farside. Lavas rise owing to the relative low density of the melt and do not possess sufficient hydrostatic head to reach the surface on the farside, except in craters in some very deep basins.

3. Methods used to probe the lunar interior

The Apollo Lunar Surface Experiments Package (ALSEP), deployed across the lunar surface by the astronauts on Apollo missions 12, 14, 15, 16, and 17, gathered much data relevant to the lunar interior. Each ALSEP installation consisted of a set of geophysical instruments connected to a central base station. The base station acted as the command center for the entire package. It received commands and transmitted data to and from Earth, and distributed power to each experiment. The astronauts also gathered a wide collection of samples from the lunar surface that were returned to Earth for analysis.

Instruments both onboard spacecraft in lunar orbit and Earth-bound also gather measurements that are useful for deciphering the Moon's internal structure. These include gravity and magnetic field data measured from orbit and laser ranges originating from Earth.

This section will review results of the active and passive seismic experiments and the heat flow experiment from ALSEP, analyses performed on samples gathered from the surface and shallow subsurface, and a variety of orbital and Earth-based measurements, and discuss interpretations of the lunar interior made from these data.

3.1 Apollo core samples

The near-surface structure of the Moon was revealed by core samples taken by the Apollo astronauts (Figure 3). Core tubes were either 2 or 4 centimeters in diameter and were pounded into the surface with a hammer. The deepest core was nearly 3m at the Apollo 17 landing site, and a total of 24 cores were collected over all six Apollo surface sites. These cores revealed that the shallowest lunar layer, known as the regolith, is a complex array of overlapping ejecta blankets resulting from meteor bombardment on the lunar surface throughout the Moon's history. This process is known as impact gardening, and results in a shallow layer of particles of varied size and texture (see section 4.1).

3.2 Gravity measurements

The Moon's internal structure can also be inferred through analyses of the lunar gravity field as measured from orbit (Figure 4). Variations in surface gravity across the Moon are caused by density heterogeneity in the subsurface, and these variations affect the position of orbiting spacecraft. First noticed during analysis of tracking data from NASA's Lunar Orbiter program in the 1960's, the Moon's gravity field has been mapped in successively higher resolution by missions such as NASA's Lunar Prospector in the 1990's, the Japanese space agency's SELENE orbiter (Selenological and Engineering Explorer) in the 2000's, and NASA's GRAIL mission (Gravity Recovery and Interior Laboratory) in the 2010's. The GRAIL mission mapped the Moon's gravity in unprecedented detail, resulting in the highest resolution gravity map of any body in the solar system, including Earth.

The biggest features resolved in the lunar gravity field are known as **mascons**, or mass concentrations. They are associated with giant impact basins and are caused by the uplift of a central plug of dense mantle material during impact, followed by the much later addition of dense mare basalt. Smaller shallow features are also resolved in the gravity data, including tectonic structures, volcanic landforms, basin rings, complex crater central peaks and simple bowl-shaped craters. Young ray craters have negative gravity anomalies because of the mass deficit associated with excavation of the crater, combined with the low density of the fallback rubble. Craters less than 200 km in diameter have negative gravity anomalies for the same reason (e.g., Sinus Iridum has a negative anomaly of −90 mGal). Volcanic domes such as the Marius hills have positive anomalies (+65 mGal), indicating support by a rigid lithosphere. The gravity signature of young, large, ringed basins, such as Mare Orientale, shows a "bull's-eye" pattern with a central positive anomaly (+200 mGal) surrounded by a ring of negative anomalies (−100 mGal) with an outer positive anomaly collar (+30 to +50 mGal).

In combination with topography data, the gravity field can also be used to infer the depth of the crust-mantle interface (known as the **moho**). The moho deflects in response to surface loads, and the resulting flexural signature contributes to the observed gravitational field. Crustal thickness largely correlates with topography, with the exception of the lunar mare regions. These areas of low elevation were resurfaced by high-density basaltic lava flows, resulting in more complex flexural signals. The average density of the highland crust calculated from GRAIL-derived crustal thickness estimates is 2250 kg/m^3.

The lunar highland crust is strong. High mountains such as the Apennines (7 km high), formed during the Imbrium collision 3.85 billion years ago, are uncompensated and are supported by a strong cool interior. The gravity data are consistent with an initially molten Moon that cooled quickly and became rigid enough to support loads such as the circular mountainous rings around the large, younger, ringed basins as well as the mascons. Even if some farside lunar basins do not show mascons, this may merely be a consequence of the greater thickness of the farside crust. The South Pole–Aitken Basin (the largest and oldest basin, age at least 4.1 billion years) is particularly significant in this respect.

3.3 Laser ranging

Additional information about the interior of the Moon can also be inferred from data gathered by the ongoing Lunar Laser Ranging (LLR) Experiment. This experiment consists of Earth-based laser ranges to an array of retroreflectors emplaced on the lunar surface 30 years ago by both U.S. and Russian missions.

A laser pulse is fired from the Earth to the Moon, where it bounces off a retroreflector and returns back to Earth (Figure 5). The round-trip travel time can be used to measure the Moon's shape and position with accuracy better than 2 centimeters. The analysis of LLR data provides a wealth of information concerning the dynamics and internal structure of the Moon.

The distances between the retroreflectors and the Earth change in part because of lunar rotation (physical librations) and tides. Values of the gravitational harmonics, the moments of inertia, the lunar Love number k_2 (which measures the tidal change in the Moon's moments of inertia and gravity), and variations in the lunar physical librations are related to the Moon's composition, mass distribution, and internal dynamics.

A range of internal structure models is compatible with the MOI values constrained by LLR. For example, a 60-km-thick lunar crust with density of 2.75 g/cm^3, a constant-density lunar upper mantle, a lower mantle with a similar change in density relative to the upper mantle, and a variable-radius iron core with density of 7 g/cm^3 produces an appropriate MOI. In this case the maximum core size is in the range of 220 to 350 km, and an increase in crustal density to 2.959 g/cm^3 raises the maximum core size to 400 km, consistent with other estimates (see Section 4.4). All layers can be adjusted in thickness and density to produce a suite of plausible lunar structure models.

For a perfectly rigid Moon, the mean direction of the lunar spin axis would be expected to precess with the Earth-Moon orbit plane. The LLR data show, however, that the true spin axis of the Moon is displaced from the expected direction. This is the result of ongoing active dissipation in the lunar interior, which has been proposed to be due in part to friction at the interface between the solid lower mantle and a fluid core.

3.4 Magnetic techniques

At present, the Moon does not possess an internally generated magnetic field. However, samples returned by the Apollo astronauts from the lunar surface retain natural remanent magnetism. In addition, orbital estimates of surface magnetic field strength reveal regions of increased magnetic intensity (Figure 6), albeit with field strengths of only about 1/100th of the terrestrial field. Based on the age dating of Apollo samples, this magnetic signature suggests that between about 3.6 and 3.9 billion years ago, there was a planetary-wide magnetic field that has now vanished. The field appears to have been much weaker both before and after this period.

Although taken from the lunar surface, these observed present-day remanent magnetic anomalies are relevant to the lunar internal structure since one interpretation is that the Moon once

possessed a lunar dipole field of internal origin. The favored mechanism is that the field was produced by dynamo action in a liquid iron core, similarly to the way Earth's magnetic field is generated. A core about 400 km in diameter could produce a field at the lunar surface with strength comparable to the observations. In early lunar history, this magnetization would be impressed into the cooling lunar crust.

An alternative interpretation however suggests that the magnetic signature may not be internally generated in origin but rather results from shock magnetization in transient fields generated following the basin-forming impacts in lunar history. This theory is supported by the observation that the largest crustal magnetizations appear to be located at or near the antipodes of the largest impact basins. In addition, some localized strong magnetic anomalies are associated with patterns of swirls – high albedo features that impart no observable topography. These swirls have likewise been suggested to form by some focusing effect of the seismic waves that resulted from the large basin-forming impacts. More work is clearly needed to substantiate this hypothesis and to understand the association of swirls and magnetic fields.

The internal structure of the Moon can also be inferred by measuring the lunar induced magnetic dipole moment. This is the residual response of the lunar interior to the sudden exposure of the Moon to a uniform magnetic field in a near-vacuum environment, which happens every month as the Moon passes through the Earth's geomagnetic tail. The external field is perturbed by an induced magnetic field caused by currents at the surface of a highly electrically conducting (iron) core, and these perturbations can be measured by orbiting spacecraft. Data gathered by the Lunar Prospector magnetometer were analyzed to conclude that the Moon likely does possess an iron-rich core, with a preferred radius of 340 ± 90km.

3.5 Heat flow

The rate at which a planetary body loses heat to space is an important indicator of the level of tectonism and volcanic activity on said planet. Two measurements of the lunar heat flow are available, as measured by the ALSEP's Heat Flow Experiment during the Apollo 15 and Apollo 17 mission's surface operations. The Heat Flow Experiment involved drilling a hole into the lunar regolith and inserting a probe that measured temperature at several depths within the hole. The rate at which temperature increases with depth provides a measure of the total heat flowing from the Moon's interior: 2.1 $\mu W/cm^2$ at the Apollo 15 site and 1.6 $\mu W/cm^2$ at the Apollo 17 site, respectively. These surface heat flow measurements are close to Earth-based estimates from microwave observations.

Unlike the Earth, which dissipates most of its heat by convective volcanism at the mid-ocean ridges, the Moon transports its heat to the surface by conduction. A lack of observed present-day active volcanism or tectonism on the Moon indicates that most of its original internal heat has been lost, so any observed heat flow must be instead predominantly due to the radioactive decay of heat-producing elements, with a small percent of the total heat flow consisting of the loss of residual heat from lunar formation.

If the Apollo heat flow measurements are considered to represent the average heat loss characteristic of the entire Moon, they can be used to provide constraints on the bulk lunar abundances of elements that release heat through radioactive decay. The heat-producing elements K, U, and Th were concentrated near the surface by differentiation during lunar formation. However the constraints on these abundances are only mild, as the distribution of heat-producing elements is not symmetric across the lunar surface.

The heat flow measurements made by Apollo could indicate bulk lunar uranium values as high as 45 ppb, over twice the terrestrial abundances. A more likely scenario is that uranium and other heat-producing elements are concentrated in the lunar crust. This is a consequence of magma crystallization. Potassium (K), rare earth elements (REE), and phosphorus (P) (KREEP), along with thorium and uranium, are among the last trace elements to crystallize from a melt. As the early molten Moon cooled, various minerals crystallized from the melt. Heavy olivines sank to the bottom, while lighter anorthosites floated to the top. The remaining incompatible trace elements probably remained molten for a much longer period of time and were eventually exposed to the surface through impact processes. The near-side concentration of KREEP may also help explain the asymmetric distribution of lunar mare.

3.6 Compositional studies

The Moon is dry, with no indigenous water having been detected at ppb levels, and lacks ferric iron (as determined by both orbital measurements and sample analyses). It is strongly depleted of volatile elements (e.g., K, Pb, Bi) by a factor of about 50 compared to the Earth, or 200 relative to primordial solar nebula abundances. Compared to the Earth, the most striking difference is in the abundance of iron that is reflected in the low lunar density. The Earth contains about 25% metallic Fe; the Moon, less than about 2–3%. However, the bulk Moon contains between 12 – 13% FeO, or 50% more than current estimates of 8% FeO in the terrestrial mantle. Along with its depletion in iron, the Moon also has a low abundance of **siderophile** or "metal-seeking" elements. These elements are extracted into metallic phases according to their metal/silicate partition coefficients during accretion. The lunar depletion of these elements has been used to argue that they have likely been segregated into a metallic core.

The other major element abundances are mostly model-dependent. Si/Mg ratios are commonly assumed to be **chondritic** (CI), although the Earth and many meteorite classes differ from this value. The lunar Mg value is generally estimated to be about 0.80, lower than that of the terrestrial mantle value of 0.89.

The Moon is probably enriched in refractory elements such as Ti, U, Al, and Ca, a conclusion consistent with geophysical studies of the lunar interior. This conclusion is reinforced by the data from the Galileo, Clementine, and Lunar Prospector missions, which indicate that the highland crust is dominated by anorthositic rocks. This requires that the bulk lunar composition contains about 5–6% Al_2O_3, compared with a value of about 3.6% for the terrestrial mantle and so is probably enriched in refractory elements (e.g., Ca, Al, Ti, U) by a factor of about 1.5 compared to the Earth. Both the Cr and O isotopic compositions are identical in the Earth and Moon, probably indicating an origin in the same part of the nebula, consistent with the single impact

hypothesis that derives most of the Moon from the silicate mantle of the impactor.

The Moon has a composition that is unlikely to have been made by any single-stage process from the material of the primordial solar nebula. The compositional differences from that of the primitive solar nebula, from the Earth, from Phobos and Deimos (almost certainly of carbonaceous chondritic composition), and from the satellites of the outer planets (rock/ice mixtures, with the exception of Io) thus call for a distinctive mode of origin (see Section 5).

3.7 Seismology

The Apollo astronauts deployed four seismometers on the lunar surface between 1969 and 1972 (Figure 7). These instruments gathered data continuously until 1977, making the Moon the only extra-terrestrial body for which extensive seismic data has been gathered.

The Moon is much less seismically active than the Earth, due to its lack of oceans and plate tectonics. Still, the Apollo network recorded several types of both naturally occurring and artificial seismic events, resulting in a total number of approximately 13,000 catalogued events over the 8-year span of the experiment. Because the Moon has no atmosphere to burn off potential impactors, there were a significant number of meteoroid impacts on the surface. The booster rockets and lunar modules from the Apollo spacecraft were also purposely impacted onto the surface after the departure of the astronauts, in part to test and calibrate the seismic array. Observed naturally occurring moonquakes include the relatively large but rare shallow moonquakes of unknown origin (similar to intra-plate earthquakes), and the relatively small but frequent deep moonquakes, (triggered with monthly periodicity by the lunar tides). Observed deep moonquakes generally had body wave equivalent magnitudes less than three, with most less than magnitude one; shallow moonquakes were larger, with the largest recorded events having magnitudes between five and 5.7. In addition, the network detected many noise-like thermal events that were associated with the large temperature fluctuations between lunar day and night.

Deep moonquakes are the most numerous type of seismic event, comprising approximately half of the event catalog. They are known to originate from distinct source regions located in a wide swath across the near side, at depths between approximately 700 and 1200 km (Figure 8). Events from a single source are periodic at monthly (tidal) periods, and exhibit high degrees of waveform similarity, likely representing repeated failure on existing fault structures at depth.

Compared to terrestrial seismograms, lunar seismic signals exhibit characteristics typical of a large degree of wave scattering and very low attenuation, due in part to the very fractured nature of the upper few hundred meters of lunar regolith. During seismic events, the Moon tends to "ring," resulting in recorded signals of extremely long duration, sometimes an hour or more, with P- and S-wave codas that mask secondary arrivals. The small number of seismic stations and lack of high-quality seismic events limited the types of analyses that could be performed. Despite these limitations, data from the Apollo passive seismic network have been extensively analyzed to reveal details on the Moon's internal structure, confirming the presence of separate crust, mantle, and core layers (Figure 9).

The detailed structure of the upper kilometer of the lunar crust was determined by two additional seismic experiments: the Active Seismic Experiment on Apollo 14 and 16, and the Lunar Seismic Profiling Experiment on Apollo 17. In both experiments, the astronauts detonated a series of small explosives on the lunar surface (Figure 10). A network of geophones then recorded the ground motions generated by these explosions. On Apollo 14 and 16, up to 19 explosions were detonated by an astronaut using a "thumper" device along a 90-meter-long geophone line. Additionally, on Apollo 16, three mortar shells were used to launch explosive charges to distances of up to 900 meters from the ALSEP. On Apollo 17, the astronauts were able to position eight explosive charges at distances of up to 3.5 kilometers from the Lunar Module, with the assistance of the Lunar Roving Vehicle. Both the Apollo 16 mortar shells and the Apollo 17 explosives were detonated by radio control after the astronauts left the lunar surface.

These experiments showed that the seismic P-wave velocity is between 0.1 and 0.3 km/s in the upper few hundred meters of the crust at all three landing sites. These velocities are much lower than observed for intact rock on Earth, but are consistent with a highly fractured material produced by the prolonged meteoritic bombardment of the Moon. At the Apollo 17 landing site, the surface basalt layer was determined to have a thickness of 1.4 km.

The lower crust and mantle seismic velocities have been estimated using the classical nonlinear inversion of compressional and shear wave arrival time readings made from the Apollo seismograms (Table 2). Shallow structure is constrained largely using surface and near-surface events (impacts and shallow moonquakes), while deep structure is constrained using mid-mantle and deeper events (deep moonquakes). Seismic velocities increase steadily down to approximately 20 km. At that depth, there is a change in velocities within the crust that probably represents the depth to which extensive fracturing, due to massive impacts, has occurred (see Figure 12 and Section 4.1). At an earlier stage of seismic data analysis, this velocity change was thought to represent the base of the mare basalts, but these are now known to be much thinner. The main section of unbroken crust from 20 to 60 km has rather uniform velocities of 6.8 km/s, corresponding to the velocities expected from the average anorthositic composition of the lunar samples.

Very few seismic rays detected by Apollo traverse the region below the deep moonquake zone. Evidence for a highly attenuating region in the deep interior such as a layer of partial melt or a fluid lunar core is implied in part by a lack of observation of seismic signals originating from the far side of the Moon (Figure 11). Since deep moonquakes are generally small, their energy cannot penetrate the attenuating region to reach the nearside Apollo array. An additional interpretation of the lack of farside signals is that the farside is aseismic, which given the other global nearside/farside asymmetries (e.g. crustal thickness, mare distribution), is not outside the realm of possibility. Further seismic exploration is needed to resolve this issue.

4. Lunar internal structure

Decades of research following the Apollo era has led to a model of the lunar interior that consists of a silicate crust and mantle, and a small iron core (Figure 1). Overlying the crust is a very thin

layer of extremely pulverized material known as the regolith, resulting from the initial heavy and continued bombardment of meteorites on the lunar surface. As discussed previously, the crust is globally asymmetric in thickness, with the nearside on average thinner than the farside. The mantle is considered to be largely homogeneous, with increases in seismic velocity and density of only a few percent from the base of the crust down to the partial melt boundary later between the mantle and core. The core itself likely consists of a fluid outer layer and a solid inner layer. This section will provide details on the structure of the lunar interior.

4.1 Regolith

The surface of the Moon is covered with a debris blanket, called the regolith, produced by the impacts of meteorites (Figure 12). It ranges in scale from fine dust to blocks several meters across. Although there is much local variation, the average regolith thickness on the maria is 4–5 m, whereas the highland regolith is about 10 m thick.

Seismic velocities are only about 100 m/s at the surface, but increase to 4.7 km/s at a depth of 1.4 km at the Apollo 17 site. The density is about 1.5 g/cm^3 at the surface, increasing with compaction to about 1.7 g/cm^3 at a depth of 60 cm. The porosity at the surface is about 50% but is strongly compacted at depth. The individual crater ejecta blankets that comprise the regolith typically range in thickness from a few millimeters up to about 10 cm, derived from the multitude of meteorite impacts at all scales. These have little lateral continuity even on scales of a few meters. Most of the regolith is of local origin: lateral mixing occurs only on a local scale so that the mare–highland contacts are relatively sharp over a kilometer or so. The rate of growth of the regolith is very slow, averaging about 1.5 mm/million years or 15 Å/year, but it was more rapid between 3.5 and 4 billion years ago during the late heavy bombardment.

Five components make up the lunar regolith: mineral fragments, crystalline rock fragments, breccia fragments, impact glasses, and agglutinates. The latter are aggregates of smaller particles welded together by glasses. They may compose 25–30% of a typical regolith sample and tend to an equilibrium size of about 60 μm. Their abundance in a sample is a measure of its maturity, or length of exposure to meteoritic bombardment. Most lunar regolith samples reached a steady state in particle size and thickness. Agglutinates contain metallic iron droplets (typically 30–100 A°) referred to as "nanophase" iron, produced by surface interaction with the solar wind during melting of the regolith by meteorite impact.

A "megaregolith" of uncertain thickness covers the heavily cratered lunar highlands. This term refers to the debris sheets from the craters and particularly those from the large impact basins that have saturated the highland crust. The aggregate volume of ejecta from the presently observable lunar craters amounts to a layer about 2.5 km thick. Earlier bombardment may well have produced megaregolith thicknesses in excess of 10 km. Related to this question is the degree of fracturing and brecciation of the deeper crust due to the large basin collisions (Figure 12). Some estimates equate this fracturing with the leveling off in seismic compression-wave velocities (v_p) to an approximately constant 7 km/s at 20–25 km depth. In contrast to the highlands, bedrock is present at relatively shallow depths (tens of meters) in the lightly cratered maria.

4.2 Crust

Various recent studies indicate that the lunar crust is approximately 34 km at the Apollo 12/14 landing sites and the average crustal thickness lies between 34 and 43 km in thickness. The farside crust averages about 15 km thicker than that of the nearside. The crust thus constitutes about 9% of lunar volume. The maximum relief on the lunar surface is over 16 km. The deepest basin (South Pole–Aitken) has 12-km relief.

The mare basalts cover 17% of the lunar surface, mostly on the nearside (Figure 13). Although prominent visually, they are usually less than 1 or 2 km thick, except near the centers of the basins. These basalts constitute only about 1% of the volume of the crust and make up less than 0.1% of the volume of the Moon.

Seismic velocities increase steadily down to around 25 km. At that depth, there is a change in velocities within the crust that probably represents the depth to which extensive fracturing due to massive impacts, has occurred (Figure 12). At an earlier stage, this velocity change was thought to represent the base of the mare basalts, but these are now known to be much thinner. The main section of the crust from approximately 20 to 40 km has rather uniform shear (S) and compression (P) wave velocities, corresponding to the velocities expected from the average anorthositic composition of the lunar samples.

4.3 Mantle

The structure of the mantle has been difficult to evaluate on account of the complexity of interpreting the lunar seismograms. From moment of inertia considerations alone we know it is largely homogeneous at least in density. The average P-wave velocity is 7.7 km/s and the average S-wave velocity is 4.45 km/s down to about 1200 km. Most models postulate a pyroxene-rich upper mantle that is distinct from an olivine-rich lower mantle beneath about a depth of 500–600 km. Seismic data are ambiguous regarding the nature of the lunar mantle below 500 km. They may be interpreted as representing magnesium-rich olivines or indicate the presence of garnet. If the latter is present, this implies that the Moon has a larger bulk aluminum content than has been predicted previously, which has important implications for reconstructing the early evolution of the Moon. However this distinction cannot be made on the basis of the Apollo seismic data alone.

The seismically active deep moonquake zone lies deep within the lower mantle at about 800–1000 km depth (Figure 9). The very low seismic attenuation observed in the outer 800 km of the mantle is indicative of a volatile-free rigid lithosphere. Solid-state mantle convection is thus extremely unlikely in the Moon.

Below about 800 km, P- and S-waves become attenuated (v_S = 2.5 km/s). P-waves are transmitted through the center of the Moon, but S-waves are missing, possibly suggesting the presence of a melt phase (Figure 11). It is unclear, however, whether the S-waves were not transmitted or were so highly attenuated that they were not recorded by the nearside Apollo array.

4.4 Core

The evidence for a metallic core is suggestive but inconclusive. As discussed previously, current (indirect) constraints on core properties arise from moment of inertia considerations, the Lunar Laser Ranging experiment, magnetic induction studies, and also from analyses of elemental abundances in mare basalts. These estimates are varied, and the presence of a lunar core (and its properties, if existent) is a topic of debate among the planetary science community.

Electromagnetic sounding data place an upper limit of a 400- to 500-km radius for a highly conducting core. The moment of inertia value of 0.3931 ± 0.0002 is low enough to require a small density increase in the deep interior, in addition to the low-density crust. Although a metallic core with a radius of about 400 km (4% of lunar volume) is consistent with the available data, denser silicate phases might be present. The resolution of these problems requires improved seismic data.

A direct seismic constraint on the size and state of the lunar core (through observation of reflected and/or converted core phases on Apollo seismograms) has not been achieved, due in part to the strong scattering of seismic energy in the lunar regolith and the limited sensitivity of the instruments. Many deep moonquake signals occurred at or just slightly above the Apollo instrument detection threshold (approximately 5.4×10^{-9} cm of ground motion at 1Hz), and if any seismic phases were observed at all, these were typically the main P- and S-wave arrivals. Since the predicted amplitudes of the lunar core phases are many times smaller, the extended coda of the primary arrivals obscured their identification on individual Apollo seismograms. However, recent application of a terrestrial seismology technique known as "array stacking" revealed the presence of several core-reflected phases, arguing strongly for a solid inner core, a fluid outer core, and a partial melt boundary layer that likely accounts for the lack of observed farside deep moonquake signals (Figure 14).

5. Implications for lunar formation and evolution

A practical model for lunar formation must result in a Moon that is consistent with the observations presented in this chapter. In addition, it must be able to explain the high value for the angular momentum of the Earth–Moon system, the strange lunar orbit inclined at 5.09° to the plane of the ecliptic, the high mass relative to that of its primary planet and the low bulk density of the Moon, much less than that of the Earth or the other inner planets. The chemical age and isotopic data revealed by the returned lunar samples added additional complexities to these classic problems because the lunar composition is unusual by either cosmic or terrestrial standards. It is perhaps not surprising that previous theories for the origin of the Moon failed to account for this diverse set of properties and that only recently has something approaching a consensus been reached.

Hypotheses for lunar origin can be separated into five categories:

1. Capture of an intact Moon from an independent orbit
2. Simultaneous Earth-Moon formation as a double planet (or "co-accretion")
3. Fission of the Moon from a rapidly rotating Earth

4. Disintegration of incoming planetesimals
5. Earth impact by a Mars-sized planetesimal and capture of the resulting debris into Earth orbit

These are not all mutually exclusive, and elements of some hypotheses occur in others. For example:

1. Capture of an already formed Moon from an independent orbit has been shown to be highly unlikely on dynamic grounds. The hypothesis provides no explanation for the peculiar composition of our satellite. In addition, it could be expected that the Moon might be an example of a common and primitive early solar system object, similar to the captured rock-ice satellites of the outer planets, particularly since the Moon's density is similar to that of primitive carbonaceous chondrites. It would however be an extraordinary coincidence if the Earth had captured an object with a unique composition, in contrast to the many examples of icy satellites captured by the giant planets.

2. Formation of the Earth and the Moon in association as a double-planet system immediately encounters the problems of differing density and composition of the two bodies. Various attempts to overcome the density problem led to co-accretion scenarios in which disruption of incoming differentiated planetesimals formed from a ring of low-density silicate debris. Popular models to provide this ring involved the breakup of differentiated planetesimals as they come within a **Roche limit** (about 3 Earth radii). The denser and tougher metallic cores of the planetesimals survived and accreted to the Earth, while their mantles formed a circum-terrestrial ring of broken-up silicate debris from which the Moon could accumulate. This attractive scenario has been shown to be flawed because the proposed breakup of planetesimals close to the Earth is unlikely to occur. It is also difficult to achieve the required high value for the angular momentum in this model. Such a process might be expected to have been common during the formation of the terrestrial planets, and Venus, in particular, could be expected to have a satellite.

3. In 1879, George Darwin proposed that the Moon was derived from the terrestrial mantle by rotational fission (Figure 15). Such fission hypotheses have been popular since they produced a low-density, metal-poor Moon. The lunar sample return provided an opportunity to test these hypotheses because they predicted that the bulk composition of the Moon should provide some identifiable signature of the terrestrial mantle. The O and Cr isotopic compositions are similar, and this is sometimes used to argue for a lunar origin from the Earth's mantle. However, other significant chemical differences remain. The Moon contains, for example, 50% more FeO and has distinctly different trace siderophile element signatures. It also contains higher concentrations of refractory elements (e.g., Al, U) and lower amounts of volatile elements (e.g., Bi, Pb). The similarity in V, Cr, and Mn abundances in the Moon and the Earth is nonunique since CM, CO, and CV chondrites show the same pattern. These differences between the chemical compositions of the Earth's mantle and the Moon are fatal to theories that wish to derive the Moon from the Earth. But perhaps more importantly, the angular momentum of the Earth–Moon system, although large, is insufficient by a factor of about 4 to allow for rotational fission. If the Earth had been spinning fast enough for fission to

occur, there is no available mechanism for removing the excess angular momentum following lunar formation.

4. One proposed modification of the fission hypothesis uses multiple small impacts to place terrestrial mantle material into orbit that sequentially accretes into a moon. However, it is exceedingly difficult to obtain the required high angular momentum by such processes because multiple impacts are random in both direction and energy, and the angular momentum they impart to the Earth over time should average out.

Most of these Moon-forming hypotheses should be general features of planetary and satellite formation and should produce Moon-like satellites around the other terrestrial planets. They either fail to account for the high angular momentum (relative to the other terrestrial planets) of the Earth–Moon system and the dry composition of the Moon, or they do not account for the differences between the lunar composition and that of the terrestrial mantle.

The single-impact hypothesis was developed to solve the angular momentum problem, but, in the manner of successful hypotheses, it has accounted for other parameters as well and has become a consensus in the lunar science community. The theory proposes that, during the final stages of accretion of the terrestrial planets, a body about the size of Mars collided with the Earth and spun out a disk of material from which the Moon formed. This giant impact theory resolves many of the problems associated with the origin of the Moon and its orbit. The following scenario is one of several possible, although restricted, variations on the theme.

In the closing stages of the accretion of the terrestrial planets from the protoplanetary disk surrounding our Sun, the Earth suffered a grazing impact with an object of about 0.10 Earth mass. This body is assumed to have been differentiated into a silicate mantle and a metallic core. Because the oxygen and chromium signatures of Earth and Moon are identical and the impact velocities are required to be low in the formation models, the impactor likely came from the same general region of the initial planet-forming nebula as the Earth.

The impactor was disrupted by the collision and the resulting debris mostly went into orbit about the Earth. Gravitational torques, due to the asymmetrical shape of the Earth following the impact, assisted in accelerating material into orbit. Expanding gases from the vaporized part of the impactor also promoted material into orbit. Following the impact, the mantle material from the impactor was accelerated, but its metallic core remained as a coherent mass and was decelerated relative to the Earth, so that it fell into the Earth within about four hours. A metal-poor mass of silicate, mostly from the mantle of the impactor, remained in orbit.

In some variants of the hypothesis, the orbiting material immediately coalesced to form a totally molten Moon. In others, it broke up into several “moonlets” that subsequently accreted to form a partly molten Moon. This highly energetic event accounts for the geochemical evidence that indicates that at least half the Moon was molten shortly after accretion. Figure 16 illustrates several stages of a computer simulation of the formation of the Moon according to one version of the single giant impact hypothesis.

Although the giant impact event vaporized much of the material, the material now in the Moon does not seem to have condensed from vapor. The extreme depletion of very volatile elements and the bone-dry nature of the Moon may be inherited from the impactor and so have been a general feature of the early inner solar nebula (all primary meteorite minerals are anhydrous) with volatiles and water added later to the Earth from near Jupiter.

Unique events are notoriously difficult to accommodate in most scientific disciplines. An obvious requirement in this model is that a suitable population of impactors existed in the early solar system. Evidence in support of the previous existence of large objects in the early solar system comes from the ubiquitous presence of heavily cratered ancient planetary surfaces, from the large number of impact basins with diameters up to 2000 km or so, and from the obliquities or tilts of the planets, all of which demand collisions with large objects in the final stages of accretion. The extreme example is that an encounter between Uranus and an Earth- sized body is required to tip that planet on its side. Thus, the possibility of many large collisions in the early solar system is well established, one of which had the right parameters to form the Moon. The single impact scenario is thus consistent with the planetesimal hypothesis for the formation of the planets from a hierarchical sequence of smaller bodies.

References

Dickey, J. O.; Bender, P. L.; Faller, J. E.; Newhall, X. X.; Ricklefs, R. L.; Ries, J. G.; Shelus, P. J.; Veillet, C.; Whipple, A. L.; Wiant, J. R.; Williams, J. G.; Yoder, C. F. (1994) Lunar Laser Ranging: A Continuing Legacy of the Apollo Program, Science Vol. 265, No. 5171, p. 482 – 490.

McKay, D. S.; Heiken, G.; Basu, A.; Blanford, G.; Simon, S.; Reedy, R.; French, B. M.; Papike, J. (1991) The lunar regolith, chapter in The Lunar Source Book, Heiken, G. H.; Vaniman, D. T.; French, B. M., editors, Cambridge University Press.

Nakamura, Y.; Latham, G. V.; Dorman, H. J. (1982) Apollo lunar seismic experiment – Final summary, Proc. Lunar Planet. Sci. Conf. 13th, 117 – 123.

Nakamura, Y. (2005) Farside deep moonquakes and deep interior of the Moon, Journal of Geophysical Research 110, doi:10.1029/2004JE002332.

Weber, R. C.; Lin, P.; Garnero, E. J.; Williams, Q.; Lognonné, P. (2011) Seismic detection of the lunar core, Science 331, 309 – 312.

Wieczorek, M. A.; Jolliff, B. L.; Khan, A.; Pritchard, M. E.; Weiss, B. P.; Williams, J. G.; Hood, L. L.; Righter, K.; Neal, C. R.; Shearer, C. K.; McCallum, I. S.; Tompkins, S.; Hawke, B. R.; Peterson, C.; Gillis, J. J.; Bussey, B. (2006) The Constitution and Structure of the Lunar Interior, Reviews in Mineralogy and Geochemistry 60, 221 – 364.

Zuber, M. T.; Smith, D. E.; Watkins, M. M.; Asmar, S. W.; Konopliv, A. S.; Lemoine, F. G.; Melosh, H. J.; Neumann, G. A.; Phillips, R. J.; Solomon, S. C.; Wieczorek, M. A.; Williams, J. G.; Goossens, S. J.; Kruizinga, G.; Mazarico, E.; Park, R.S.; Yuan, D. (2013) Gravity Field of the Moon from the Gravity Recovery and Interior Laboratory (GRAIL) Mission, Science 339, 668 – 671 (2013).

Figure Captions

Figure 1: Schematic cross-section of the Moon showing the approximate depths of layering inferred using various geophysical methods. The nearside is to the left. The thickness of the crust is shown for a pole-to-pole profile at 0 and 180° longitude; the nearside crust is known to be thinner than the farside crust. The source regions of natural moonquakes (dots) detected by the Apollo seismometers (squares) have been projected onto the nearside hemisphere as a function of depth and latitude (see Section 3.7) (figure reproduced from Wieczorek et al., 2006).

Figure 2: Schematic cross-section of the Moon in the equatorial plane showing the displacement of the Moon's center of mass towards Earth (figure left), due to the presence of a thicker farside crust (figure right). The crustal thickness is exaggerated for clarity. An equipotential surface is indicated with a dashed line (figure reproduced from "The Moon" chapter in the previous edition of the Encyclopedia of the Solar System).

Figure 3: (left) Core sample being taken by Apollo 12 astronaut Alan Bean at the Bench Crater site (photo AS12-49-7243 from the Apollo Image Archive). (right) Apollo 15 core sample during analysis at the Lunar Sample Laboratory Facility, NASA Johnson Space Center (photo S79-37062 from Apollo Image Archive).

Figure 4: Bouguer gravity anomaly map from the GRAIL lunar gravity model GL0420A. The map is a Molleweide projection centered on 270°E longitude, with the nearside on the right and farside on the left (figure reproduced from Zuber et al., 2013.)

Figure 5: (left) The Lunar Laser Ranging Station at the University of Texas McDonald Observatory. Photo by Randall L. Ricklefs. (right) Laser retroreflector installed on the lunar surface by the Apollo 11 astronauts (photo AS11-40-5952 from the NASA Apollo Archive).

Figure 6: Total magnetic field strength at the surface of the Moon as derived from the Lunar Prospector electron reflectometer experiment, which was in orbit around the Moon during the years 1998 – 1999 (figure courtesy of M. Wieczorek).

Figure 7: (left) Map of the lunar near side (15° increments of latitude and longitude) showing the locations of the four seismometers that comprised the Apollo Passive Seismic Experiment. From west: Apollo 12, 14, 15, and 16. (right) Photograph of the Apollo 16 seismometer as installed on the lunar surface. It is covered with a mylar shield that was intended to thermally protect the instrument. Other instruments from the Apollo Lunar Surface Experiments Package can be seen in the background, as well as the central station that telemetered data continuously to Earth (photo AS16-113-18347 from the NASA Apollo Archive).

Figure 8: Map of the lunar near side (15° increments of latitude and longitude) showing the nominal epicenter locations of the deep moonquake source regions (blue squares) detected by the Apollo seismic stations (red circles). Farside source regions (outer black circle) are projected on the near side. The deep moonquakes are roughly constrained to a wide swath trending northeast-southwest across the entire nearside of the Moon.

Figure 9: Schematic cross-section of the Moon showing the crust, mantle, and core layers inferred through analyses of the Apollo seismic data. The Apollo station locations and seismically active regions are indicated; arrowheads show a sample of meteoroid impact locations (figure reproduced from Nakamura et al., 1982).

Figure 10: (left) The Apollo 16 mortar package mounted on its base. The cable running off to the left connects the experiment to the ALSEP Central Station. The red flag at the top of the mast provided a visual warning for the crew to steer clear when driving the Lunar Rover (photo AS16-113-18378 from the NASA Apollo Archive). (right) Apollo Lunar Module Pilot Edgar Mitchell walks along the geophone line during the Apollo 14 mission, operating the "thumper" (photo AS14-67-9374 from the NASA Apollo Archive).

Figure 11: Schematic cross section of the Moon showing the bounding seismic rays for shear wave shadows from the deep attenuating region. The direction to Earth is indicated. Small squares denote the Apollo seismic station locations (Apollo 12 and 14 are approximately co-located, so only one square is shown for clarity). The crosses mark the locations of hypothetical deep moonquake hypocenters for which the seismic rays to a station at a corner of the triangular station network graze the lower mantle, in which shear waves are severely attenuated. For events in Zone A, clear shear wave arrivals may be observed at all three corners of the network, i.e., none of the seismic stations are in the S wave shadow. For events in Zone B, clear shear wave arrivals may be observable at two corners of the network, i.e., one corner of the array is in the S wave shadow. For events in Zone C, clear shear wave arrivals may be observable only at one corner of the network, i.e., two corners of the array are in the S wave shadow. For events in Zone D, no clear S wave arrivals are observable at all three corners of the network, i.e., all corners of the array are in the S wave shadow (figure reproduced from Nakamura, 2005).

Figure 12: Schematic cross-section of the upper 25 km of the lunar surface, illustrating the effects of large-scale cratering on the structure of the lunar crust (figure reproduced from the Lunar Source Book).

Figure 13: A composite full-Moon photograph that shows the contrast between the heavily cratered highlands and the smooth, dark basaltic plains of the maria. Mare Imbrium is prominent in the northwest quadrant. The dark, irregular, basalt-flooded area on the west is Oceanus Procellarum. Mare Crisium is the dark circular basalt patch on the eastern edge (figure courtesy of UCO/Lick Observatory, photograph L9).

Figure 14: Schematic meridional cross-section of the Moon showing the approximate distribution of deep moonquakes (red circles) and the radii of physical layers in the deepest lunar interior, as resolved from recent re-analyses of the Apollo seismic data (figure reproduced from Weber et al., 2011).

Figure 15: Artist's rendition of the fission theory of lunar formation, in which the Moon was formed from the mantle of a hot, early Earth. In this theory, the molten Earth rotates rapidly, causing a blob of material to spin out, which later rounded into the Moon. The Pacific Ocean

basin is a popular site of choice for origin (figure reproduced from https://sites.google.com/site/parkviewastro/lunar-formation/the-fission-theory).

Figure 16: A computer simulation of the origin of the Moon by a glancing impact of a body approximately the same size of Mars with the early Earth. This event occurred about 4.5 billion years ago during the final stages of accretion of the terrestrial planets. By that time, both the impactor and the Earth had differentiated into a metallic core and rocky silicate mantle. Following the collision, the mantle of the impactor is ejected into orbit. In this simulation, the metallic core of the impactor clumps together and falls into the Earth within about four hours. Most terrestrial mantle material ejected by the impact follows a ballistic trajectory and is eventually re-accreted by the Earth. The metal-poor, low-density Moon is thus derived mainly from the silicate mantle of the impactor (figure courtesy A. G. W. Cameron).

Tables

moons	radius (km)	density (g/cm^3)	satellite-to-parent mass ratio
Europa	1561	3.014	1/39544
Moon	1738	3.344	1/81
Io	1818	3.529	1/21256
Callisto	2410	1.834	1/17575
Titan	2576	1.880	1/4225
Ganymede	2634	1.942	1/12825
materials			
wood (pine)	-	0.500	-
water	-	1.000	-
stone (granite)	-	2.700	-
metallic iron	-	7.874	-

Table 1: Radius, density, and satellite-to-parent mass ratio of the largest 5 satellites in the Solar System, sorted by radius. The densities of several common Earth materials are given for comparison.

depth (km)	v_p (km/s)	v_s (km/s)	ρ (g/cm^3)
0.0	1.0	0.5	2.6
1.0	1.0	0.5	2.6
1.0	3.2	1.8	2.7
15.0	3.2	1.8	2.7
15.0	5.5	3.2	2.8
40.0	5.5	3.2	2.8
40.0	7.7	4.4	3.3
238.0	7.7	4.4	3.3
238.0	7.8	4.4	3.4
488.0	7.8	4.4	3.4
488.0	7.6	4.4	3.4
738.0	7.6	4.4	3.4
738.0	8.5	4.5	3.4
1257.1	8.5	4.5	3.4
1257.1	7.5	3.2	3.4
1407.1	7.5	3.2	3.4
1407.1	4.1	0.0	5.1
1497.1	4.1	0.0	5.1
1497.1	4.3	2.3	8.0
1737.1	4.3	2.3	8.0

Table 2: Lunar seismic P- and S-wave velocity and density structure with depth.

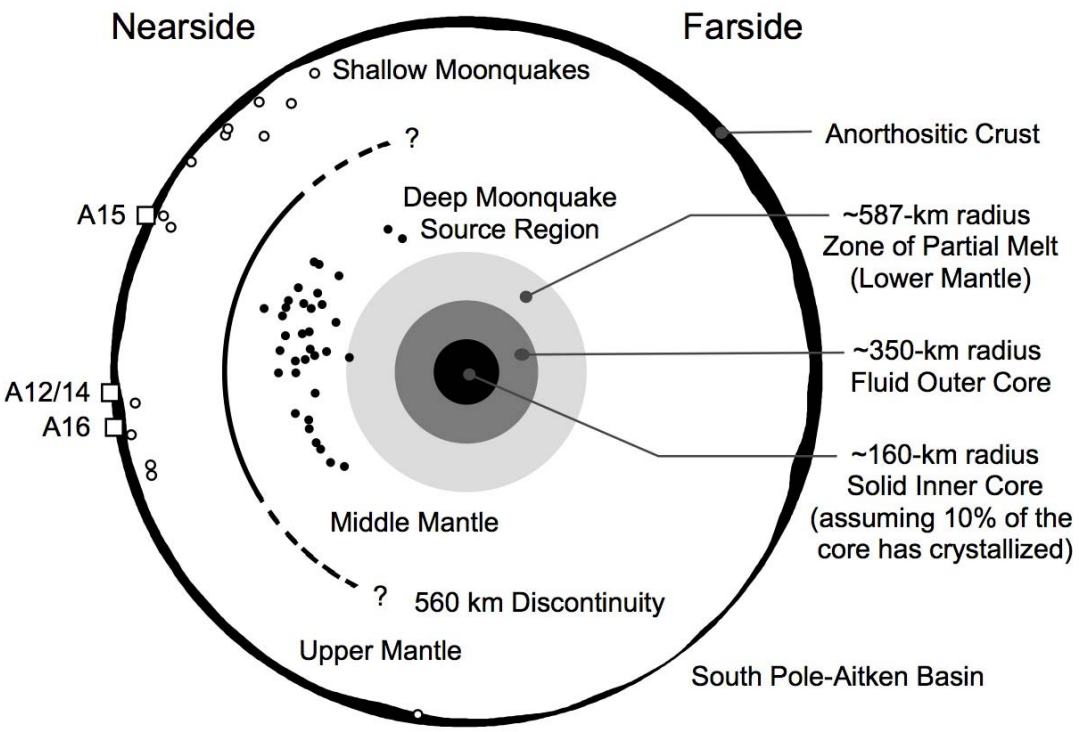
Nearside
Farside
Shallow Moonquakes
?
Deep Moonquake
Source Region
A15
A12/14
A16
Anorthositic Crust
~587-km radius
Zone of Partial Melt
(Lower Mantle)
~350-km radius
Fluid Outer Core
~160-km radius
Solid Inner Core
(assuming 10% of the
core has crystallized)
Middle Mantle
?
560 km Discontinuity
Upper Mantle
South Pole-Aitken Basin

Figure 1

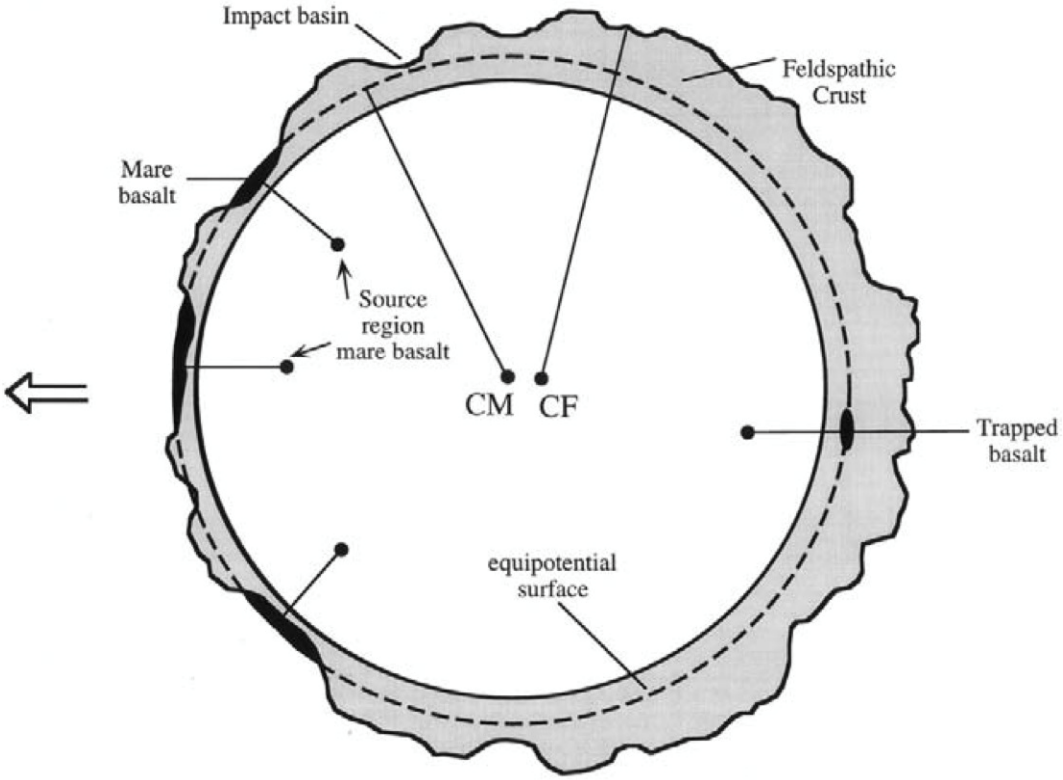
Impact basin
Feldspathic Crust
Mare basalt
Source region mare basalt
CM
CF
Trapped basalt
equipotential surface

Figure 2

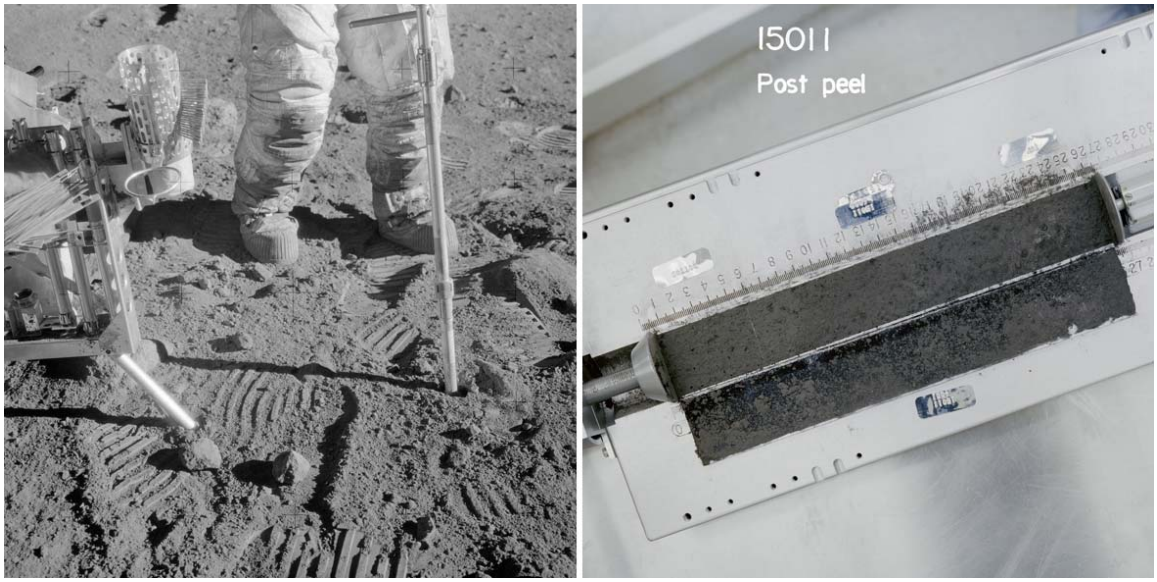

Figure 3

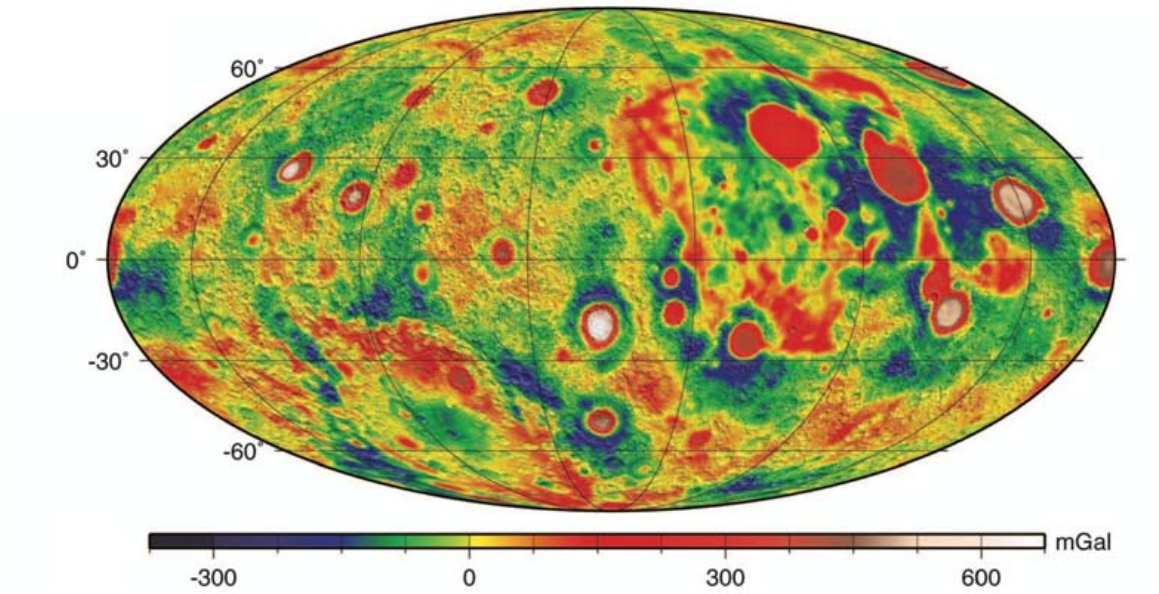

Figure 4

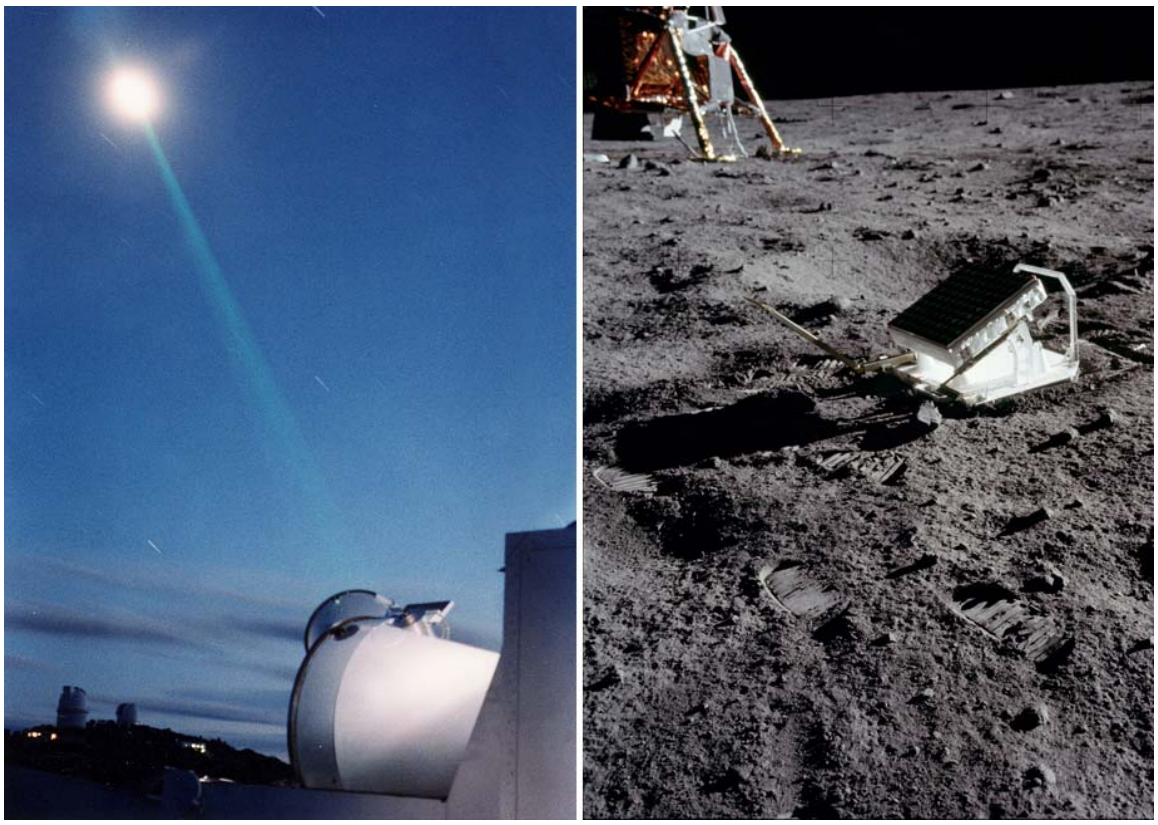

Figure 5

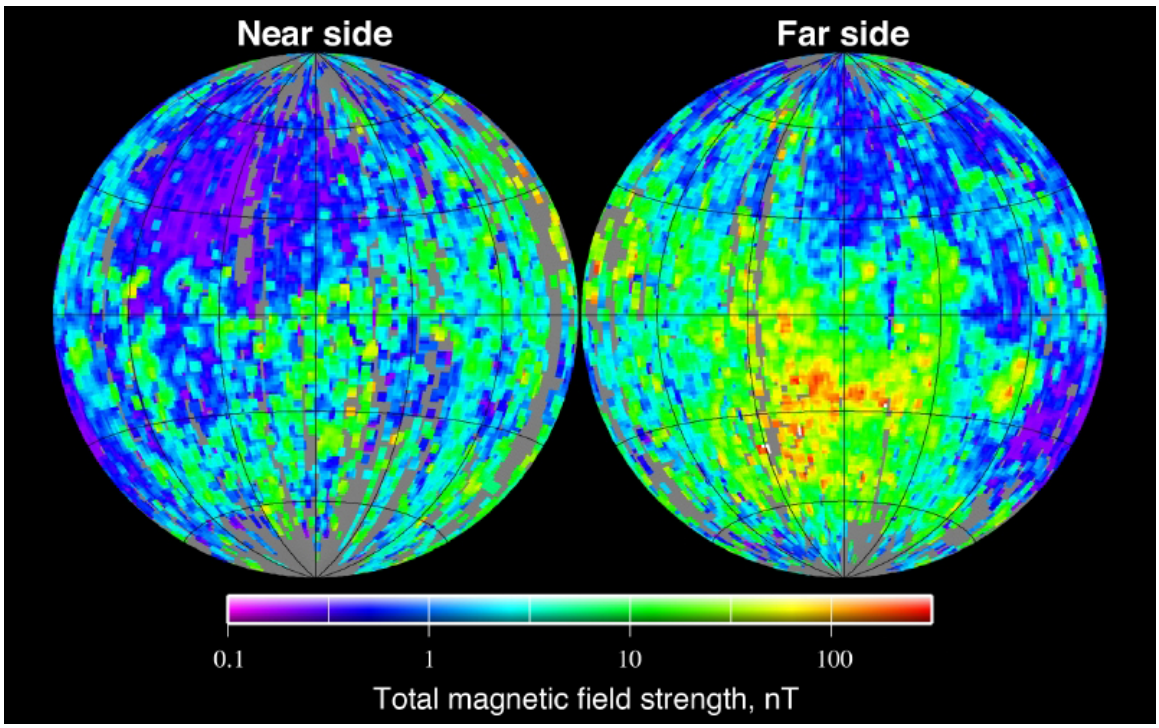
Near side
Far side
0.1
1
10
100
Total magnetic field strength, nT

Figure 6

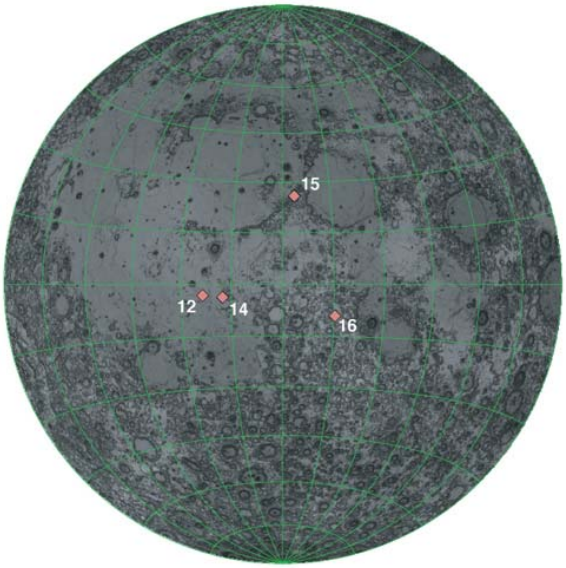

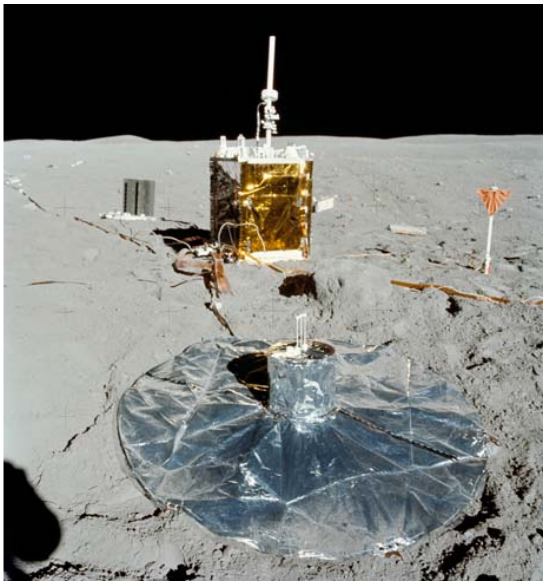

Figure 7

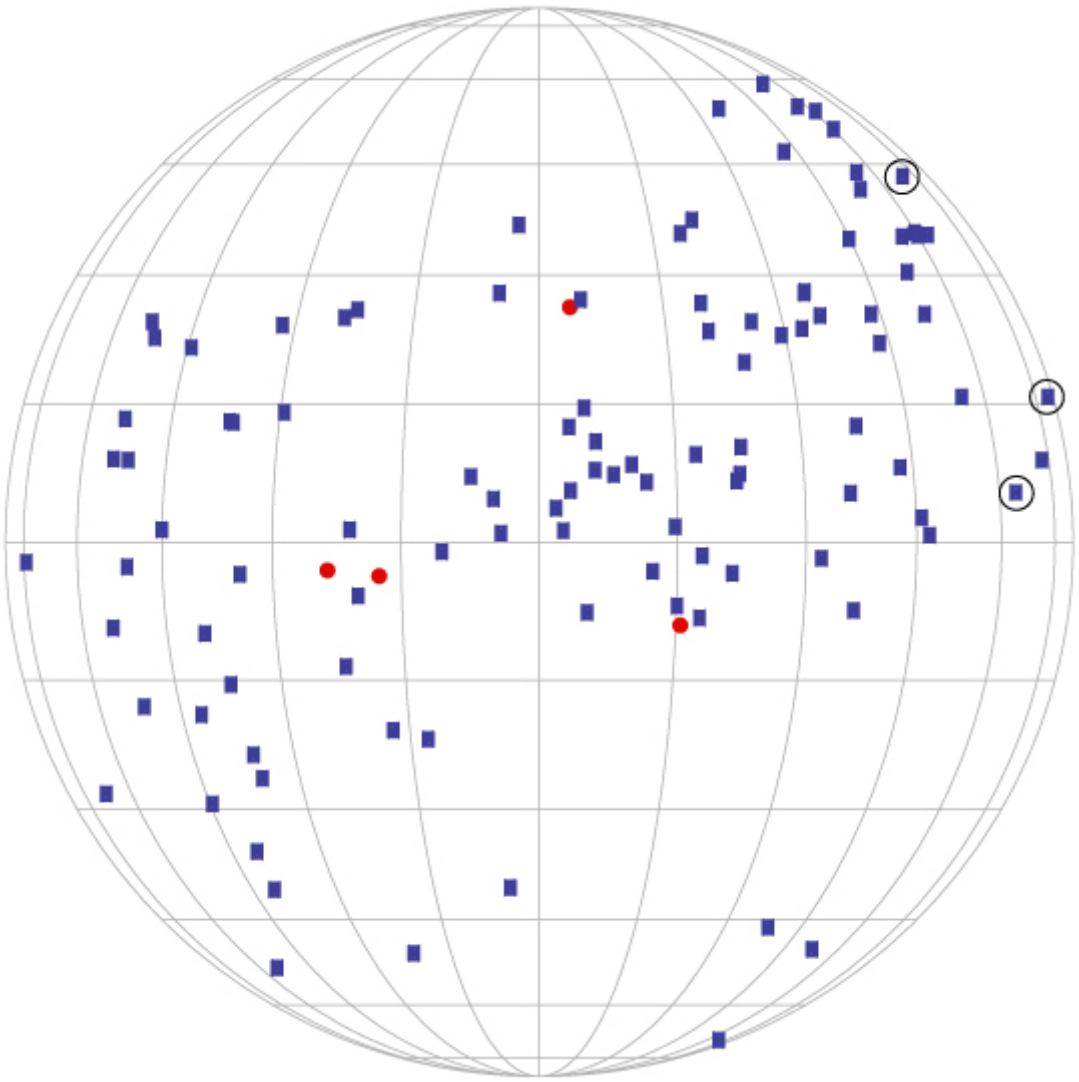

Figure 8

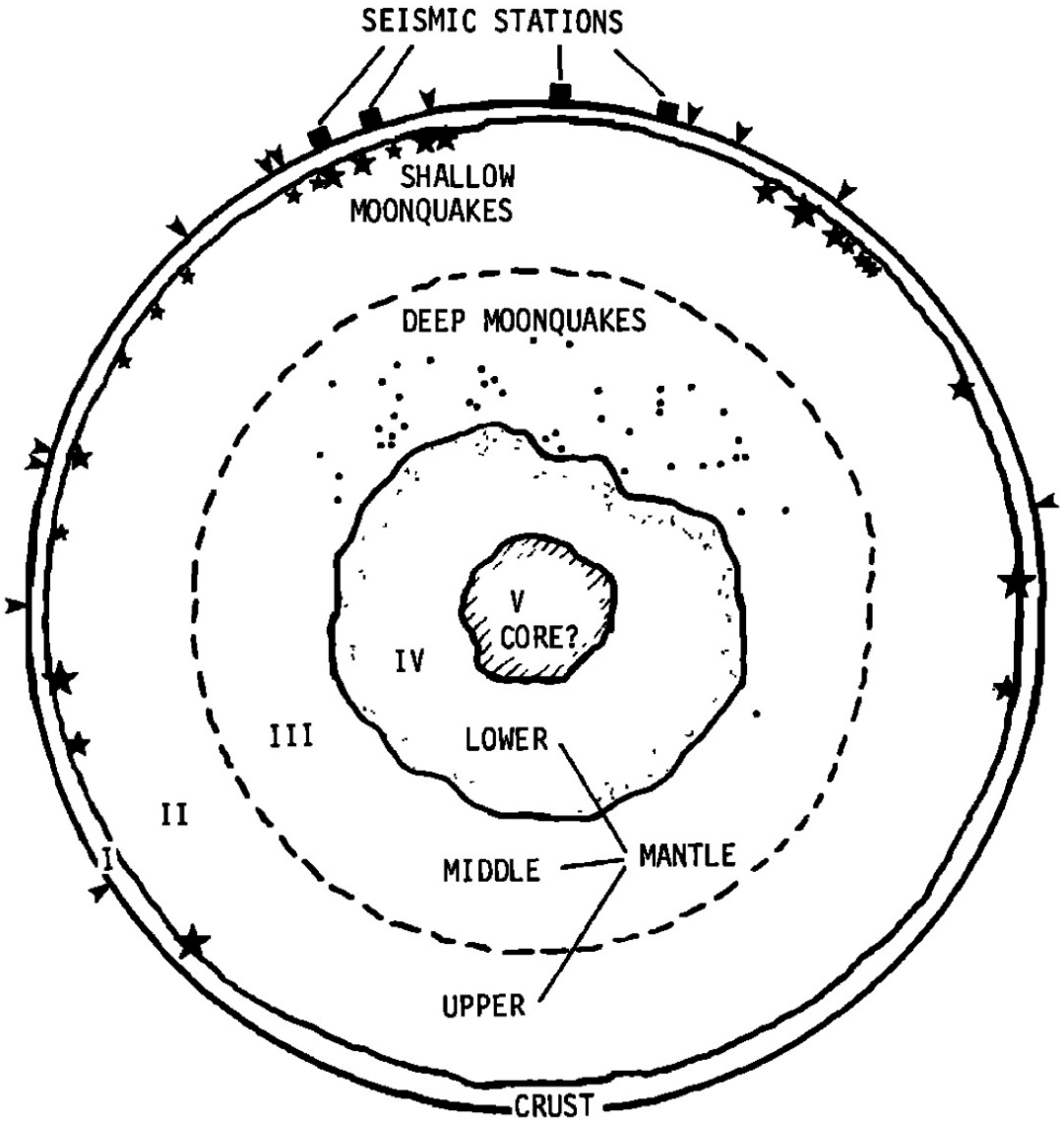
SEISMIC STATIONS
SHALLOW
MOONQUAKES
DEEP MOONQUAKES
V
CORE?
IV
III
LOWER
II
I
MIDDLE
MANTLE
UPPER
CRUST

Figure 9

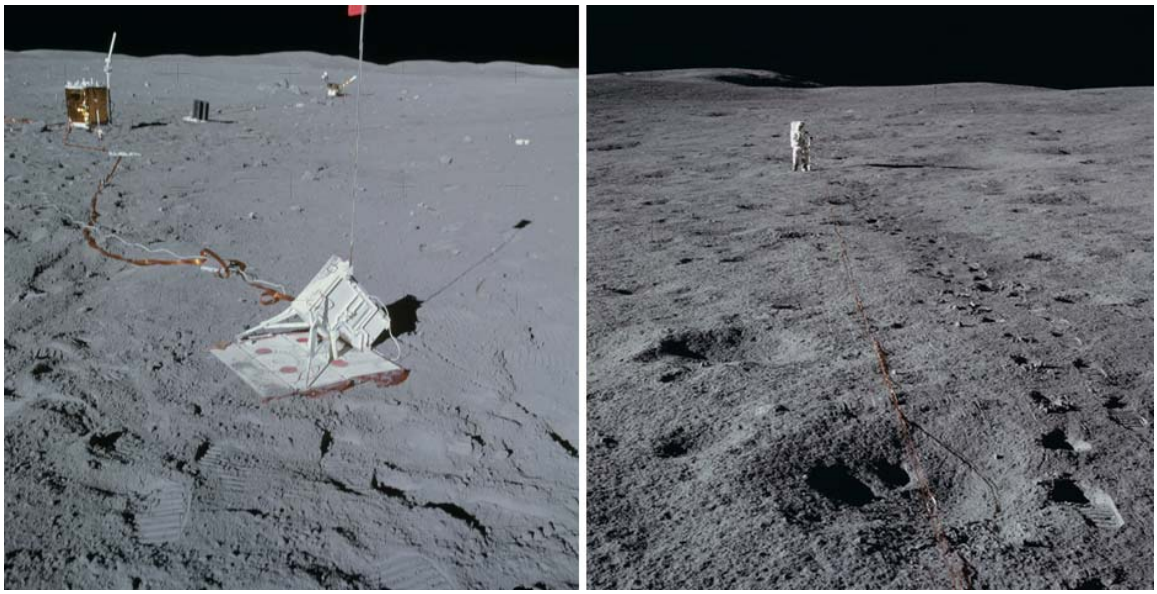

Figure 10

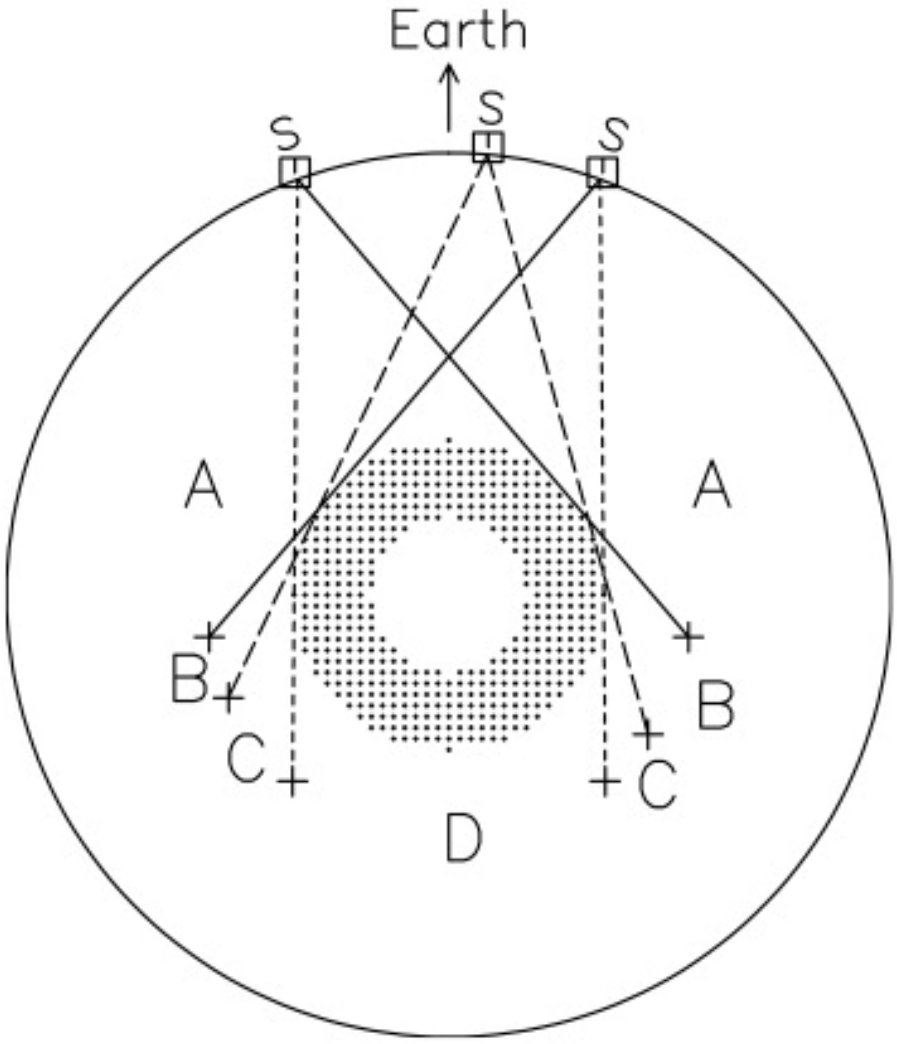

Figure 11

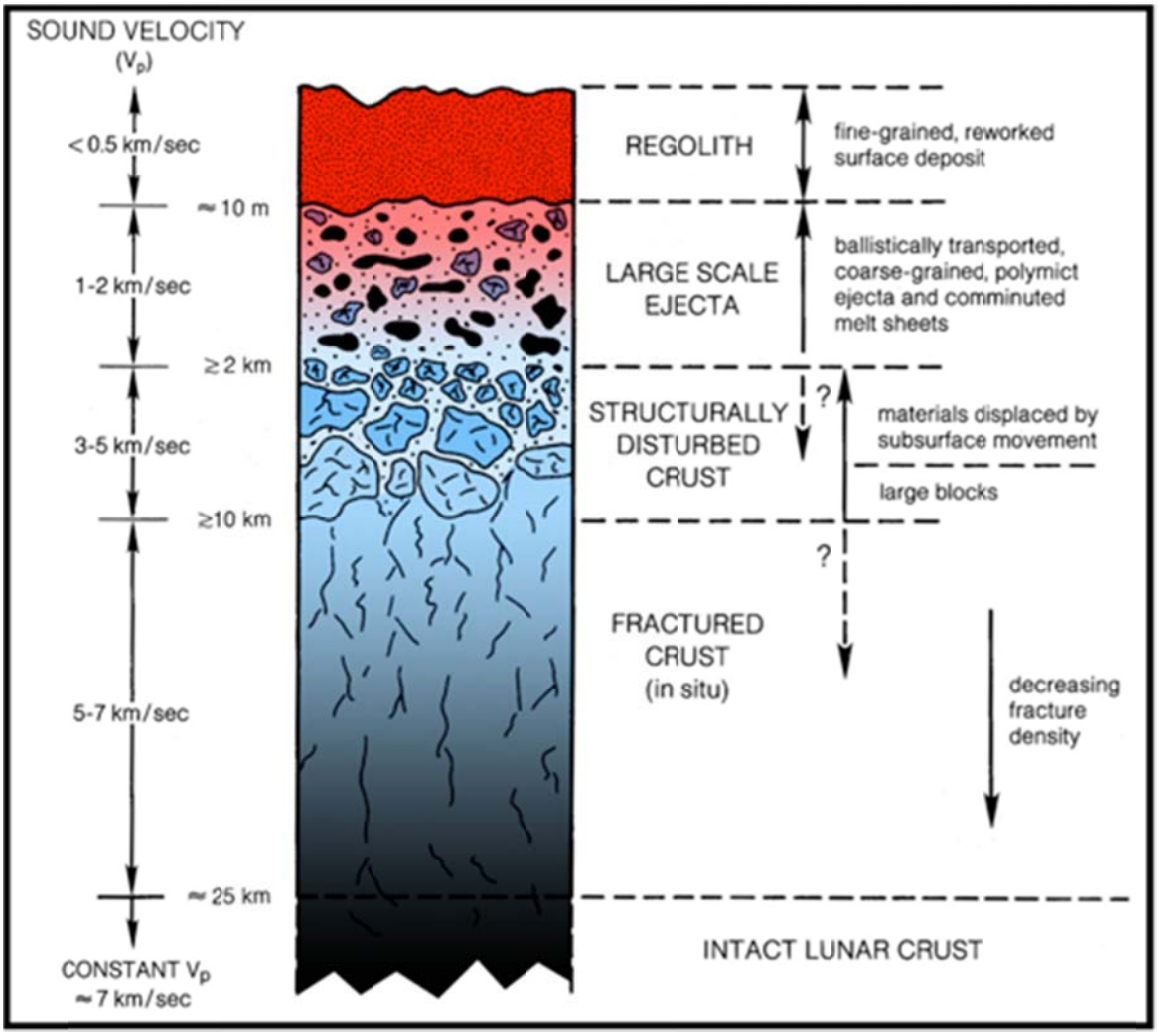
SOUND VELOCITY
(V_p)
< 0.5 km/sec
≈ 10 m
1-2 km/sec
≥ 2 km
3-5 km/sec
≥10 km
5-7 km/sec
≈ 25 km
CONSTANT V_p
≈ 7 km/sec
REGOLITH
fine-grained, reworked surface deposit
LARGE SCALE EJECTA
ballistically transported, coarse-grained, polymict ejecta and comminuted melt sheets
STRUCTURALLY DISTURBED CRUST
?
materials displaced by subsurface movement
large blocks
?
FRACTURED CRUST (in situ)
decreasing fracture density
INTACT LUNAR CRUST

Figure 12

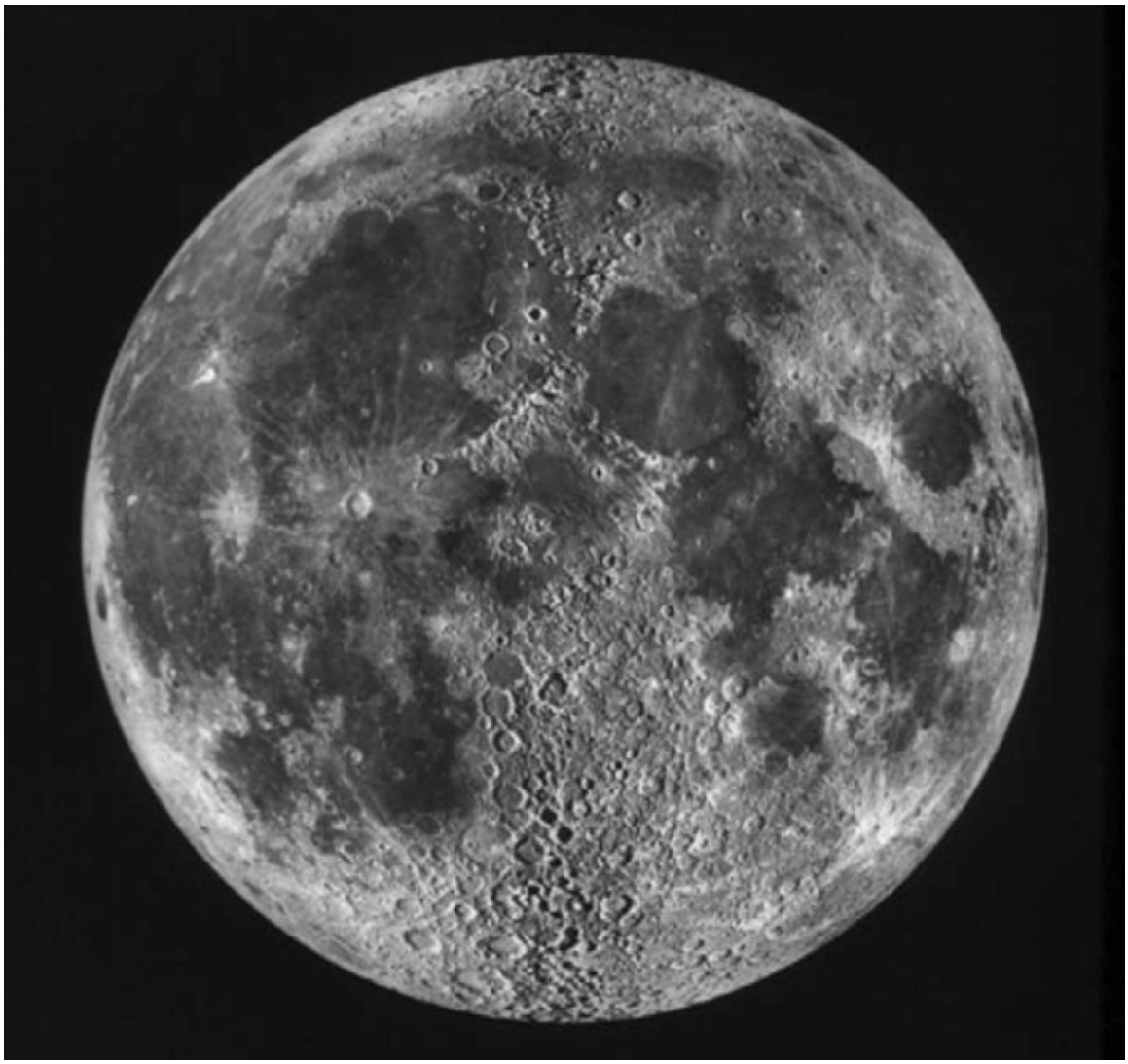

Figure 13

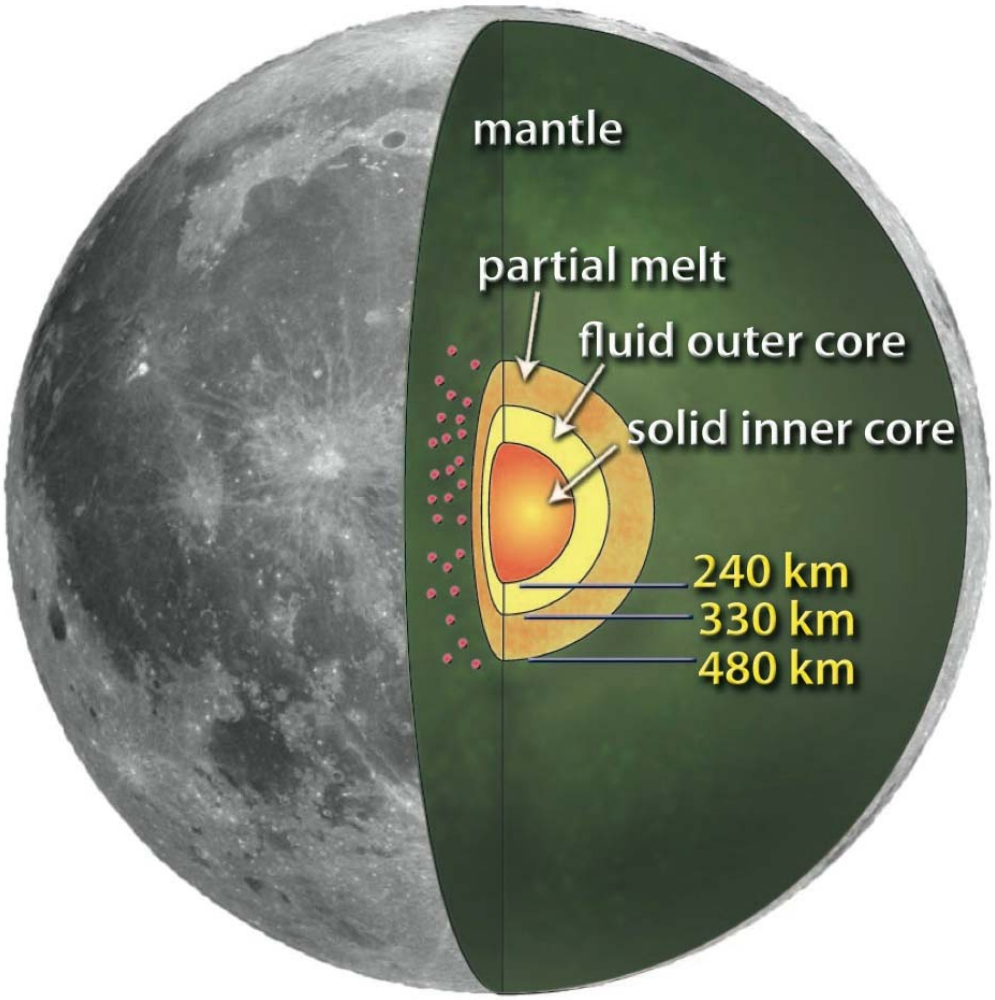
mantle
partial melt
fluid outer core
solid inner core
240 km
330 km
480 km

Figure 14

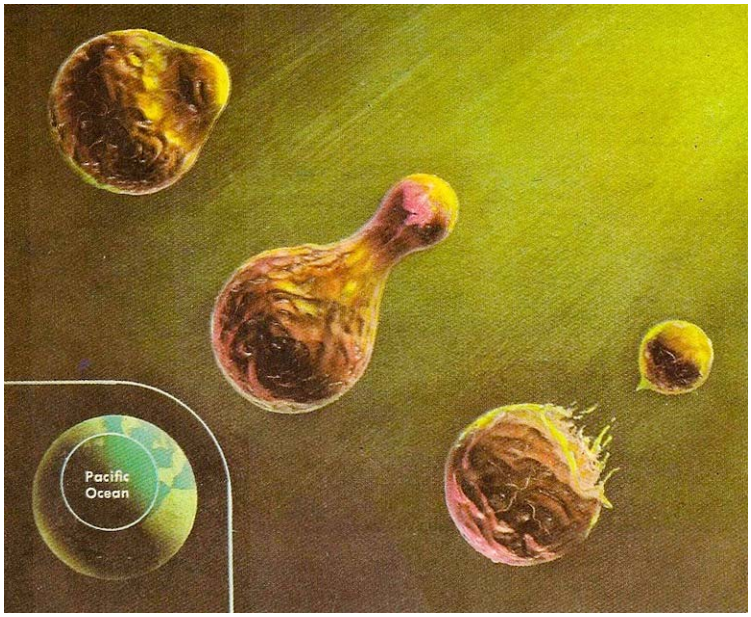

Figure 15

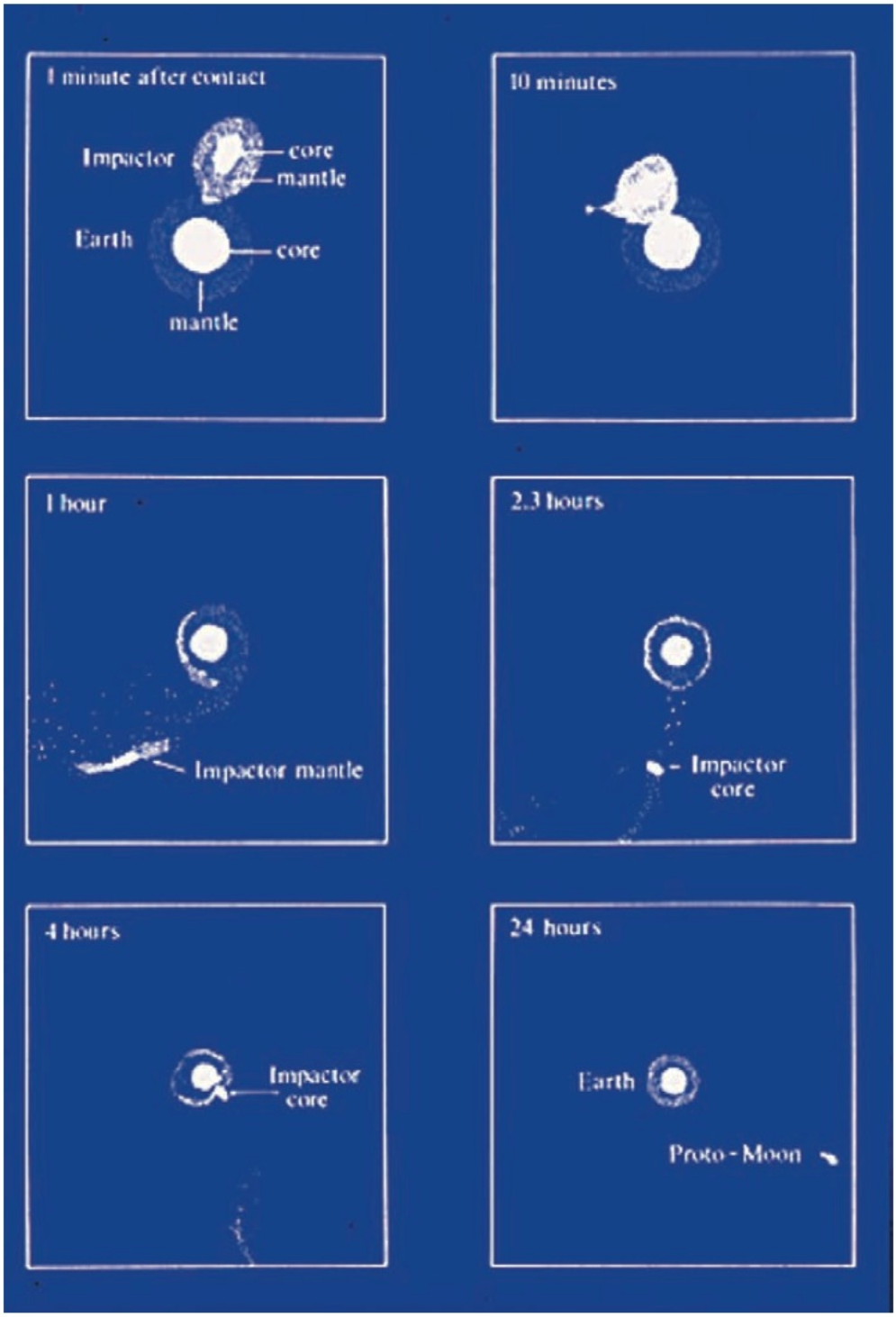
1 minute after contact
Impactor
core
mantle
Earth
core
mantle
10 minutes
1 hour
Impactor mantle
2.3 hours
Impactor
core
4 hours
Impactor
core
24 hours
Earth
Proto-Moon

Figure 16